

MODELING HYDROGEN-INDUCED FRACTURE AND CRACK PROPAGATION IN HIGH STRENGTH STEELS

MOHSEN DADFARNIA¹
University of Illinois at Urbana-
Champaign, USA

AKIHIDE NAGAO¹
JFE Steel Corporation,
Japan

BRIAN P. SOMERDAY¹
Southwest Research Institute,
USA

PHILLIP E. SCHEMBRI
Los Alamos National Laboratory,
USA

JAMES W. FOULK, III
Sandia National Laboratories,
USA

KEVIN A. NIBUR
Hy-Performance Material Testing,
USA

DORIAN K. BALCH
Sandia National Laboratories,
USA

ROBERT O. RITCHIE¹
University of California, Berkeley,
USA

PETROS SOFRONIS¹
University of Illinois at Urbana-
Champaign, USA

¹ International Institute for Carbon-
Neutral Energy Research (I²CNER),
Japan

ABSTRACT

We investigate hydrogen-induced crack initiation and subcritical crack propagation in high strength steels by addressing hydrogen transport and interaction with material deformation. Our experiments demonstrate that hydrogen reduces the fracture resistance of single-notched bend specimens of a lath martensitic steel while changing the morphology of the fracture surfaces from microvoid coalescence in the absence of hydrogen to a mixture of “quasi-cleavage” and intergranular. We modeled the onset of fracture in this steel by assuming that failure occurs by dislocation pile-ups against high angle grain boundaries whose strength is assumed to be reduced by hydrogen. The model reproduces the experimentally measured reduction of the fracture strength of the bend specimens as a function of the hydrogen charging pressure. We also present a model for subcritical crack propagation and arrest under sustained load in a hydrogen gaseous environment. The numerical results for a model high strength steel show that the velocity vs. stress intensity factor (V-K) curve exhibits the typical stages I and II. Interestingly, this model suggests that the existence of the two stages is explained solely by stress-driven diffusion of hydrogen.

INTRODUCTION

Deployment of high strength martensitic steels in hydrogen applications is limited by the reduction of their fracture resistance in hydrogen environments. This reduction is usually characterized by a change in the mode of fracture from ductile microvoid coalescence to brittle-like intergranular or transgranular

failure. Thus if high strength steels are to be inserted in designs for hydrogen applications, development of predictive models that define safe operating conditions is required.

In this paper, we study the phenomena of hydrogen-induced crack initiation and subcritical crack propagation in high strength steels accounting for the hydrogen interaction with the material elastoplastic deformation. We use the physical-based statistical micro-mechanical approach of Novak et al. [1] along with weakest-link statistics to identify the fracture initiation site and predict the fracture resistance of a lath martensitic steel in hydrogen. Next we present a model of hydrogen-induced crack propagation under sustained load in a gaseous environment applicable to high strength steels failing by stress-controlled fracture.

HYDROGEN-INDUCED FAILURE OF A LATH MARTENSITIC STEEL

Our experiments demonstrate that hydrogen reduces the strength of a modified AISI 4140 tempered lath martensitic steel [2,3]. Single edged notched bend (SENB) samples were charged under 31 and 138 MPa hydrogen pressures at 250 °C for 21 days to obtain homogeneously charged specimens with different amounts of hydrogen concentrations. Before charging, the specimens, shown schematically in Fig. 1, were zinc plated to prevent hydrogen loss after cooling down to room temperature and during testing. They were then tested in air at room temperature under displacement load control until fracture. The fracture load is reported in terms of the nominal bending stress $\sigma_{nom} = 6Fz / a^2$ where F is the applied force per unit specimen thickness, z is the moment arm, and a is the uncracked ligament.

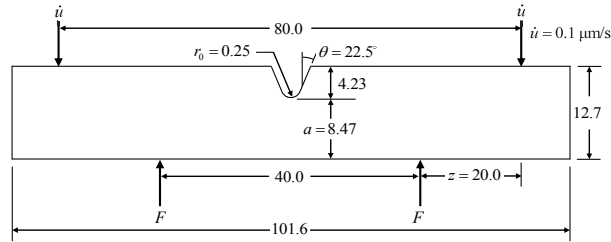


Figure 1. Schematic of SENB specimen loaded under displacement control. The failure load is measured in terms of the nominal stress $\sigma_{nom} = 6Fz / a^2$, the maximum stress in an un-notched beam of height a .

Following Novak et al. [1] and based on our experimental observations [2,3], we assume that fracture initiates by decohesion at high angle boundaries (prior austenite grain boundaries, packet and block boundaries) from the combined effect of hydrogen induced-reduction of the boundary strength and the increased stress the boundary experiences because of dislocation pile-ups.

Statistical model of fracture

We assume that the macroscopic brittle fracture behavior of the material is governed by weakest-link statistics [4]. Following Novak et al. [1], we calculate the total survival probability Φ of the material volume V according to the weakest link statistics as

$$1 - \Phi = \exp\left[-N \int_0^V \int_0^\sigma g(S) dS dV\right], \quad (1)$$

where N is the number of boundaries per unit volume that participate in the decohesion process and $\int_0^\sigma g(S) dS$ is the fraction of boundaries with interfacial strength less than the local maximum principal stress σ . We determine the interfacial strength of the boundaries through the Smith model [5]:

$$\frac{l}{d} S^2 + \tau_{eff}^2 \left[1 + \frac{4}{\pi} \frac{\tau_0}{\tau_{eff}} \sqrt{\frac{l}{d}}\right]^2 = \frac{\pi E \gamma_{eff}}{(1-\nu^2)d}, \quad (2)$$

where l is the size of a nucleating crack, d is the dislocation pile up length, τ_0 is the friction stress, $\tau_{eff} = \tau_e - \tau_0$ is the effective stress which is the difference between the applied shear stress $\tau_e = \sigma_e / \sqrt{3}$ and the friction stress τ_0 , σ_e is the effective stress, E is Young's modulus, ν is Poisson's ratio, and $2\gamma_{eff}$ is the effective fracture energy per unit area associated with the separation of the boundaries.

We consider that $2\gamma_{eff}$ consists of the reversible work of separation $2\gamma_{int}$ and the plastic work of separation γ_p accompanying the decohesion event such that $2\gamma_{eff} = 2\gamma_{int} + \gamma_p$ [6]. To account for the hydrogen effect on boundary decohesion, we assume that lattice hydrogen and hydrogen trapped at grain boundaries reduces the reversible work of separation according to the thermodynamic theory of Hirth and Rice [7]. In addition, following Jokl *et al.* [6], we assume that the plastic work of separation is a very steep function of the reversible work. This is an additional and indirect effect of hydrogen on decohesion, namely through the reduction of the attendant plastic work by reducing the reversible work.

Simulation of hydrogen-induced fracture initiation

The charging conditions determine the initial state of hydrogen distribution in the SENB specimen. Since the specimens were zinc-plated, we assume that the total hydrogen amount in the specimen does not vary with time after charging. The main trapping sites for the lath martensitic steel under consideration are dislocations, cementite particles, lath boundaries, and high angle boundaries. The binding energies of hydrogen to dislocations, cementites, lath boundaries and high angle boundaries are obtained from the literature as 30, 10.9, 30, and 47.4 kJ/mol, respectively [8–10]. Based on our experimental measurements of the dislocation density as a function of the plastic strain and the assumption that there is one hydrogen atom trapped per atomic plane

threaded by a dislocation, we considered the associated trap density to increase linearly with plastic strain from $N_T^{(D)} = 3.31 \times 10^{23}$ traps/m³ in the absence of strain to 1.13×10^{25} traps/m³ at 2% plastic strain, and remain constant for larger strains. The trap density of high angle boundaries is taken equal to 10^{23} sites/m³ [1,11]. The trap densities for lath boundaries and cementites are chosen to be 2.5×10^{25} sites/m³. The lath boundary and carbide densities are obtained such that the calculated total hydrogen concentrations at 31 and 138 MPa hydrogen charging pressure are close to those determined experimentally through thermal desorption analysis, i.e. 28.4 and 42.8 appm for 31 and 138 MPa charging pressure, respectively [2,3]. The diffusion coefficient is $D = 1.5 \times 10^{-8}$ m²/s.

The flow stress σ_e of this steel as a function of plastic strain ε^p is described by $\sigma_e = \sigma_0(1 + \varepsilon^p / \varepsilon_0)^n$, where $\sigma_0 = 1090$ MPa, $n = 0.03$, $\varepsilon_0 = \sigma_0 / E$, and $E = 200$ GPa. The size of a nucleating crack l and the dislocation pile up length d in Eq. (2) are assumed to be equal to the block size h_B which ranges from 0.3 to 2.7 μ m. The friction stress was taken $\tau_0 = 10^{-3} \mu$, where μ is the shear modulus. The number density of high angle boundaries that participate in the decohesion events is taken as $N = 2 \times 10^{13}$ /m³ which is assumed to be 1% of the density of high angle boundaries. The effective fracture work, γ_{eff} , in the absence of hydrogen was 23 J/m² [4] and reduced in the presence of hydrogen as described by Novak et al. [1].

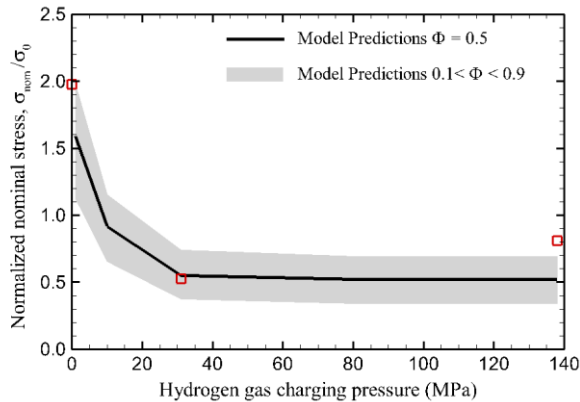


Figure 2. Normalized nominal stress σ_{nom} / σ_0 at fracture as a function of charging hydrogen pressure for the modified 4140 lath martensitic steel. The experimental data for the uncharged and hydrogen charged steels at 31 and 138 MPa are also shown on the figure.

The solution to the coupled hydrogen diffusion initial/boundary-value problem and elastoplastic boundary problem during the displacement loading of the SENB specimen was obtained through finite element analysis [1,12]. The calculated stress and hydrogen concentration at each integration point was used

to calculate the hydrogen effect on the effective work of fracture and the probability of failure according to Eq. (1). We designated the notch root normalized nominal stress at failure probability $\Phi = 50\%$ for the entire specimen as the fracture stress.

Figure 2 shows the fracture stress for the modified AISI 4140 tempered lath martensitic steel. Experimental data for uncharged and hydrogen charged specimens at 31 MPa and 138 MPa charging hydrogen pressures are superposed on the graph. The results show that the model successfully predicts the effect of hydrogen on fracture.

MODELING SUBCRITICAL CRACK GROWTH

The preferred fracture mode in hydrogen containment components is subcritical cracking. Hence, understanding the phenomenology of subcritical crack propagation can enable the development of appropriate design criteria and thus help mitigate hydrogen embrittlement in structural materials. In this section, we present a model for subcritical crack propagation for high strength steels for the case when fracture is stress-controlled.

Crack propagation model

Following Ritchie, Knott, and Rice [13], we assume that crack advances when the tensile opening stress over a characteristic distance l^* ahead of the crack tip is larger than the material fracture strength. However, unlike in the RKR model in which the fracture strength is constant, in our model we assume that the fracture strength reduces with hydrogen concentration [14]. This assumption is consistent with the results presented in Fig. 2 as well as with other works [1–3] which showed that the fracture load decreases with increasing hydrogen concentration.

The crack growth process according to our model evolves as follows: under constant load, hydrogen diffuses in the region ahead of the crack tip. As the local hydrogen concentration in the neighborhood of the crack tip increases, the corresponding local material fracture strength reduces. However, the crack does not grow until the fracture strength is lower than the opening stress over the entire characteristic distance l^* ahead of the crack tip. When this criterion is satisfied, the crack advances. The process of hydrogen accumulation and subsequent crack extension continues on until the crack propagation criterion cannot be satisfied, which coincides with crack arrest.

Numerical simulation

We simulate subcritical crack growth in a real-life wedge opening load (WOL) specimen by the finite element method. We solved the coupled initial/boundary-value problem of hydrogen diffusion and elastoplastic deformation over the entire WOL specimen domain under plane strain conditions. The height of the specimen is $2H = 55.4$ mm, the width $W = 59.6$ mm, and the initial crack length $a_0 = 26.8$ mm. Because of symmetry, we analyzed only the upper half of the specimen. We assumed that the specimen

was initially hydrogen-free and that hydrogen entered the specimen only through the crack faces which were maintained always in equilibrium with hydrogen gas as new surface was created upon crack propagation. We imposed zero flux boundary conditions on all other external surfaces of the domain of analysis. We used the nodal release technique for crack propagation. Once the criterion for crack growth was met, we released the nodes along the crack line over the characteristic distance l^* . The nodes were released one by one starting from crack tip node so that the process resembles the real crack growth process. During nodal release, we assumed that the hydrogen concentration in the bulk of the specimen did not change. After the completion of the release process, we imposed the concentration boundary condition on the newly released nodes and switched on the hydrogen diffusion. The hydrogen diffusion and accumulation ahead of the crack tip continued until the criterion for crack propagation was met again.

We considered a model high strength steel with yield stress $\sigma_0 = 1500$ MPa, hardening exponent $n = 0.1$, Young's modulus $E = 200$ GPa, Poisson's ratio $\nu = 0.3$, and hydrogen diffusion coefficient $D = 2 \times 10^{-8}$ m²/s. Whereas the model accounts for the effect of hydrostatic stress gradient on hydrogen diffusion and hydrogen-induced lattice dilatation, for the sake of simplicity, hydrogen trapping was ignored. For the characteristic distance for fracture, we assumed $l^* = 100$ μm which represents a length scale for a typical grain boundary. Three curves for the dependence of fracture strength on hydrogen concentration were considered (Fig. 3a), where the parameter c_0 is 1 appm. Note that the curves were so constructed that the fracture strength for all three cases is the same at normalized hydrogen concentration $c/c_0 = 0$ and 6. Whereas the curve labeled as linear is a straight line connecting the two points, the quadratic curve is a second-order polynomial with slope equal to zero at $c/c_0 = 6$ and the cubic one is a cubic polynomial with first and second derivatives equal to zero at $c/c_0 = 6$.

The specimen was initially loaded by increasing the displacement associated with bolt loading of the specimen to a level representing stress intensity factor $K_I^0 = 90$ MPa $\sqrt{\text{m}}$. Then the displacement was kept constant in time as the simulation of hydrogen transport and crack propagation was carried out. At time $t = 0$ and while the specimen was loaded at K_I^0 , the hydrogen diffusion was switched on. After some time, which represents an incubation period for the hydrogen to diffuse and reduce the material strength over the distance l^* ahead of the crack tip, the crack started to propagate and the simulation was continued till the crack was arrested. As the crack propagates the stress intensity factor decreases since the bolt loading displacement is constant. The arrest took place when the hydrogen concentration near the crack tip reached a steady-state, i.e. the hydrogen concentration over the characteristic distance did not change after the arrest. Consequently, the fracture strength could not be further degraded and crack extension ceased.

During the simulation, we calculated the crack size and the associated stress intensity factor as a function of time. From these data, we calculated the crack growth rate as a function of stress intensity factor (V-K curve). The results for the three strength curves shown in Fig. 3a are depicted in Fig. 3b. The crack propagation rates exhibit the typical characteristic stages I and II of subcritical cracking. Interestingly, both stage I and stage II of the V-K curve are captured without resorting to a different mechanism of crack propagation for each stage. As shown from Fig. 3, the shape of the strength vs. concentration curves influences the V-K curves both in stage I and stage II.

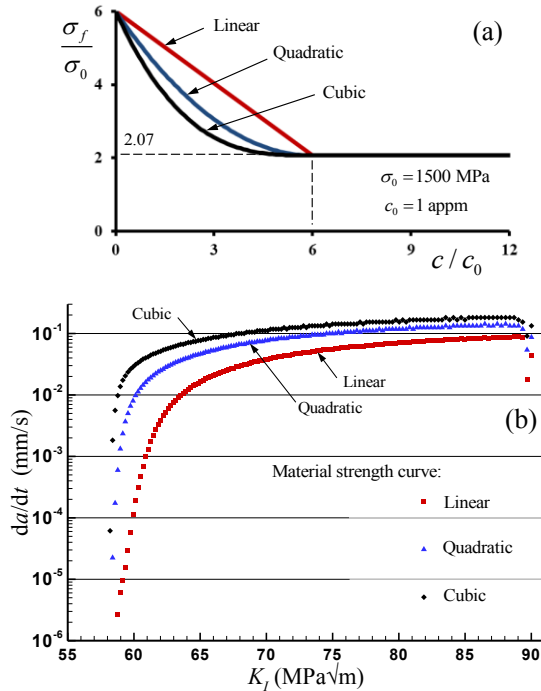


Figure 3. (a) Fracture strength for the model high strength material as a function of local hydrogen concentration, (b) V-K curves for the corresponding fracture strength relationships. All specimens were bolt loaded at $K_I^0 = 90 \text{ MPa}\sqrt{\text{m}}$ prior to hydrogen gas exposure. The fracture characteristic distance was assumed $l^* = 100 \mu\text{m}$. The parameter $\sigma_0 = 1500 \text{ MPa}$ is the yield stress of the material and $c_0 = 1 \text{ appm}$ is a normalizing concentration [14].

CONCLUSIONS

We presented a statistical micro-mechanical model for hydrogen-induced crack initiation for a lath martensitic steel. The model is based on hydrogen-induced reduction of the cohesive energy of high angle boundaries and elevation of local stress experienced by the boundaries due to impingement of dislocation

pile ups. The model predictions for the fracture strength are in excellent agreement with experimental data for a tempered lath martensitic steel. A second model for hydrogen-induced stress-controlled crack propagation was also presented in which hydrogen was assumed to reduce the fracture strength over a characteristic distance ahead of the crack tip. With such a simple but physically based assumption for high strength steels, simulated crack propagation V-K curves were found to exhibit stage I and stage II behavior. Significantly, both stages are explained by the same physics which is diffusion controlled crack propagation.

ACKNOWLEDGEMENTS

M.D., A.N., B.P.S., R.O.R. and P.S. gratefully acknowledge the support of the International Institute for Carbon-Neutral Energy Research (WPI-I²CNER), sponsored by the World Premier International Research Center Initiative (WPI), MEXT, Japan. P.E.S. acknowledges support from Los Alamos National Laboratory, an affirmative action/equal opportunity employer, operated by Los Alamos National Security, LLC, for the National Nuclear Security Administration of the U.S. Department of Energy under contract DE-AC52-06NA25396. J.W.F. and D.K.B. acknowledge support from Sandia National Laboratories, a multi-program laboratory managed and operated by Sandia Corp., a wholly owned subsidiary of Lockheed Martin Corp., for the US Department of Energy's National Nuclear Security Administration under Contract DE-AC04-94AL85000.

REFERENCES

- [1] Novak, P., Yuan, R., Somerday, B. P., Sofronis, P., and Ritchie, R. O., 2010, "A Statistical, Physical-Based, Micro-Mechanical Model of Hydrogen-Induced Intergranular Fracture in Steel," *Journal of the Mechanics and Physics of Solids*, **58**(2), pp. 206–226.
- [2] Nagao, A., Smith, C. D., Dadfarnia, M., Sofronis, P., and Robertson, I. M., 2012, "The Role of Hydrogen in Hydrogen Embrittlement Fracture of Lath Martensitic Steel," *Acta Materialia*, **60**(13-14), pp. 5182–5189.
- [3] Nagao, A., Martin, M. L., Dadfarnia, M., Sofronis, P., and Robertson, I. M., 2014, "The Effect of Nano-Sized (Ti,Mo)C Precipitates on Hydrogen Embrittlement of Tempered Lath Martensitic Steel," *Acta Materialia*, **74**, pp. 244–254.
- [4] Lin, T., Evans, A. G., and Ritchie, R. O., 1986, "A Statistical Model of Brittle Fracture by Transgranular Cleavage," *Journal of the Mechanics and Physics of Solids*, **34**(5), pp. 477–497.
- [5] Smith, E., 1966, "The Nucleation and Growth of Cleavage Microcracks in Mild Steel," *Proceedings of Conference on Physical Basis of Yield and Fracture*, A.C. Stickland, ed., Institute of Physics and Physics Society, Oxford, pp. 36–46.
- [6] Jokl, M. L., Vitek, V., and McMahon Jr., C. J., 1980, "A Microscopic Theory of Brittle Fracture in Deformable Solids: A Relation between Ideal Work to Fracture and Plastic Work," *Acta Metallurgica*, **28**(11), pp. 1479–1488.
- [7] Hirth, J. P., and Rice, J. R., 1980, "On the Thermodynamics of Adsorption at Interfaces as It Influences Decohesion," *Metallurgical Transactions A*, **11**(9), pp. 1501–1511.
- [8] Itakura, M., Kaburaki, H., Yamaguchi, M., and Okita, T., 2013, "The Effect of Hydrogen Atoms on the Screw Dislocation Mobility in Bcc Iron: A First-Principles Study," *Acta Materialia*, **61**(18), pp. 6857–6867.
- [9] Hong, G. W., and Lee, J. Y., 1983, "The Interaction of Hydrogen and the Cementite-Ferrite Interface in Carbon Steel," *Journal of Materials Science*, **18**(1), pp. 271–277.
- [10] Takai, K., and Abe, N., 2013, "Identification of Hydrogen Desorption Peak Temperatures,

- Binding Energies, and Occupation Ratios at Vacancies, Dislocations and Grain Boundaries in Iron and Steel,” *International Hydrogen Energy Development Forum 2013, Kyushu University, Fukuoka, Fukuoka*, pp. 29–36.
- [11] Hirth, J. P., 1980, “Effects of Hydrogen on the Properties of Iron and Steel,” *Metallurgical Transactions A*, **11**(6), pp. 861–890.
- [12] Sofronis, P., and McMeeking, R. M., 1989, “Numerical Analysis of Hydrogen Transport near a Blunting Crack Tip,” *Journal of the Mechanics and Physics of Solids*, **37**(3), pp. 317–350.
- [13] Ritchie, R. O., Knott, J. F., and Rice, J. R., 1973, “On the Relationship between Critical Tensile Stress and Fracture Toughness in Mild Steel,” *Journal of the Mechanics and Physics of Solids*, **21**(6), pp. 395–410.
- [14] Dadfarnia, M., Somerday, B. P., Schembri, P. E., Sofronis, P., Foulk, J. W., Nibur, K. A., and Balch, D. K., 2014, “On Modeling Hydrogen-Induced Crack Propagation under Sustained Load,” *JOM*, **66**(8), pp. 1390–1398.